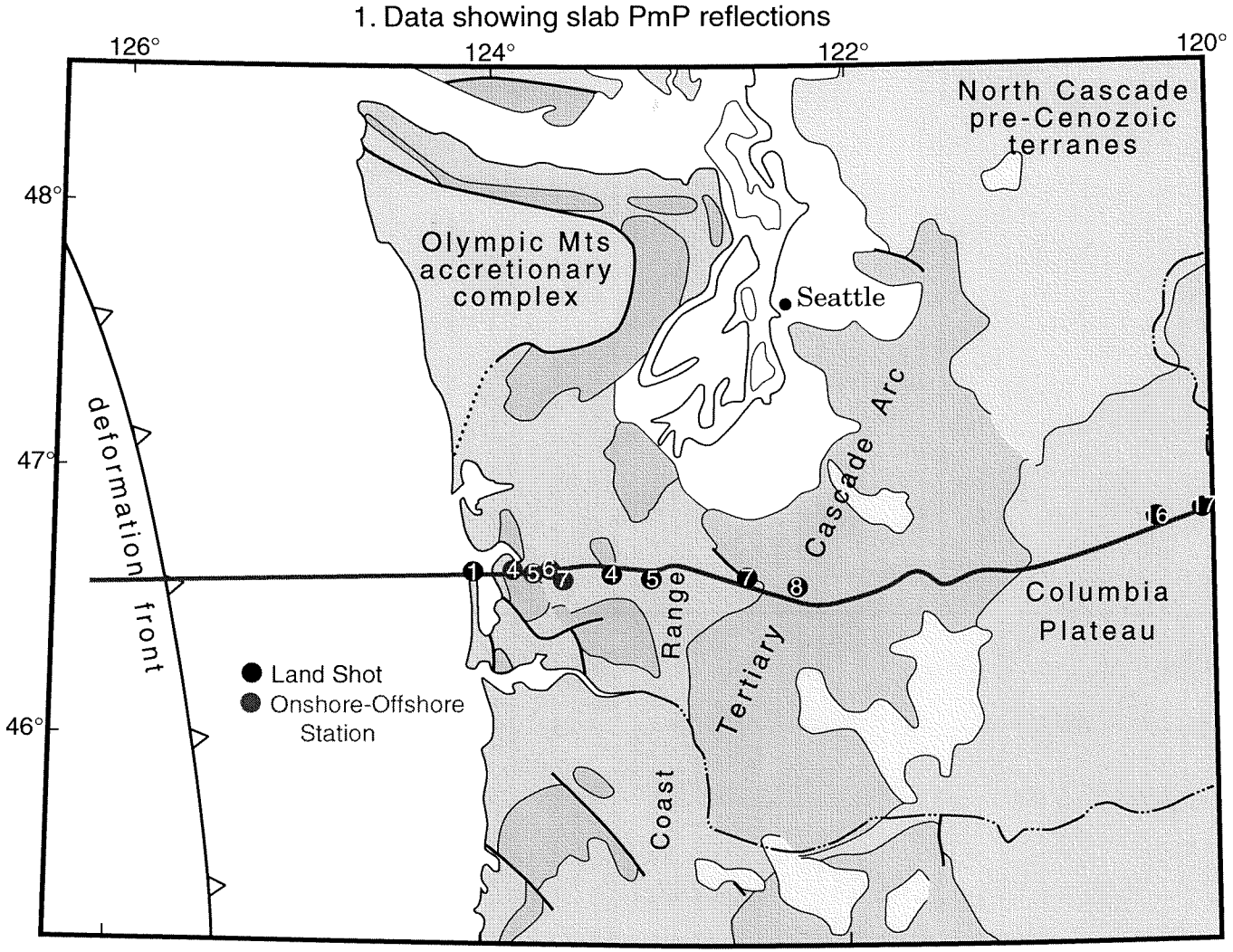

Figure 1. This figure shows the locations of the reciever or shot gathers of Figures 2-8. The data shown in Figures 2-8 are focused on secondary arrivals (reflections) because there is very little ambiguity in picking the first arrivals (primarily Pg). Thus not all the data are included. Ocean bottom seismometer (OBS) data are not included because only first-arrival traveltimes (Pg and Pn) were used from those data to construct the model in the oceanic crust offshore (because the crust is thin offshore, there is turning-ray coverage throughout the oceanic crust, providing good velocity control). The data are divided into those showing evidence for the descending slab, and those used to constrain the thickness of the continental crust. All data are shown at reduced time (6.0 km/s), and are windowed to highlight wide-angle reflections. Reflection travel times were fit to within 0.15s, and first arrivals were fit to a root mean squared (RMS) misfit of 0.10s.

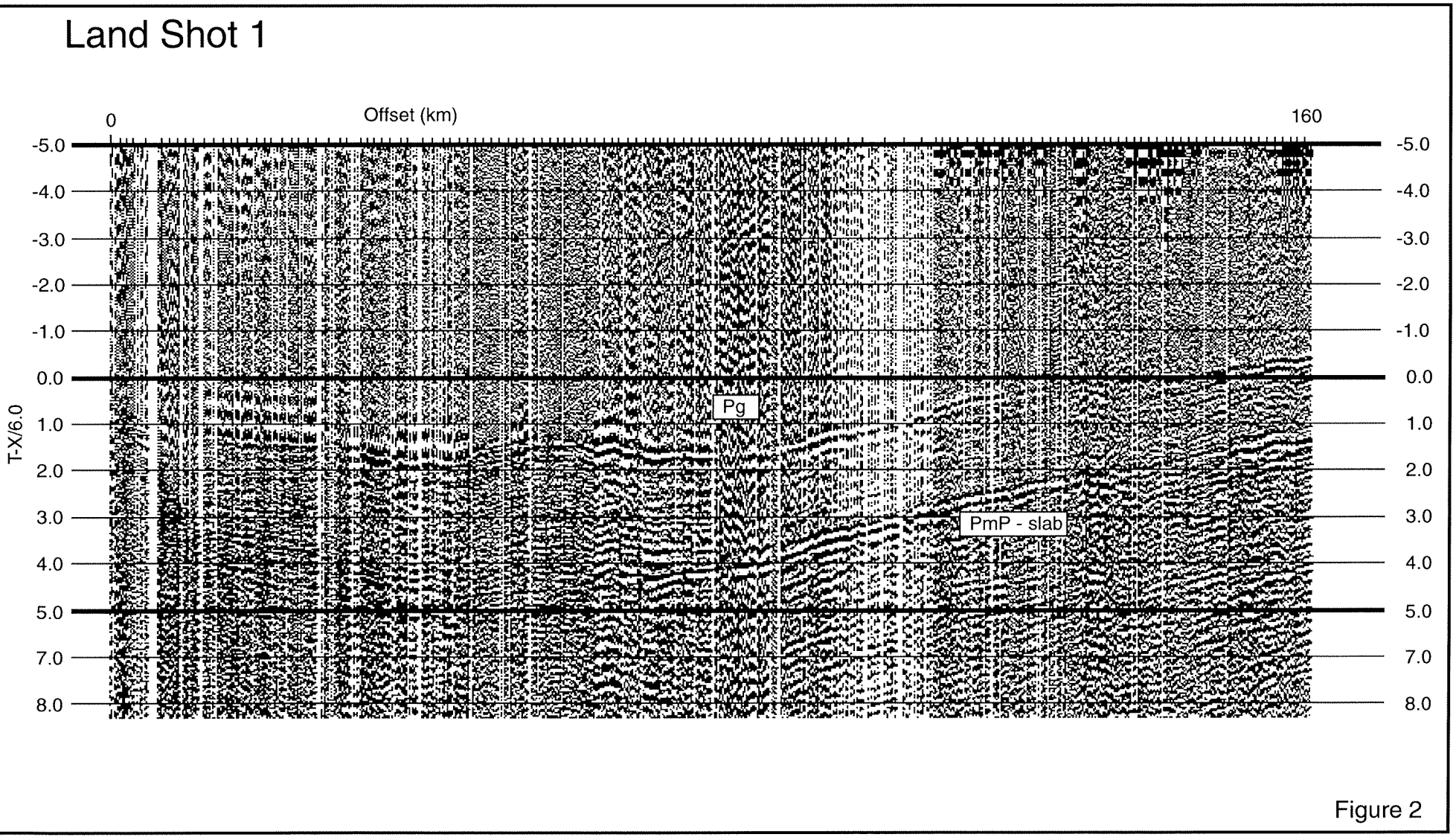
Land Shot 1
0
Offset (km)
160
-5.0
-4.0
-3.0
-2.0
-1.0
0.0
1.0
2.0
3.0
4.0
5.0
7.0
8.0
T-X/6.0
Pg
PmP - slab

Figure 2

Figure 2. Shot gather showing a wide-angle reflection from the Juan de Fuca slab. Using these data and including the other gathers shown in subsequent figures, we assessed the seismic velocity of the crust and upper mantle along the southwest Washington transect using two complementary methods. A finite-difference tomographic inversion method was used to analyze refracted arrivals traveling through the upper crust (Pg). We then extended our velocity model downward into the lower crust and descending Juan de Fuca slab by employing a finite-difference technique to forward model the propagation of seismic energy down to, and back up from, a reflecting interfaces at depth. By incorporating the inverted solution for upper-crustal velocity in our grid, we were able to accurately model the effects of near-surface upper-crustal structures (i.e., basins) on the arrival times of secondary arrivals. The techniques described here were also discussed in detail by Parsons et al. (1996).

The shallow fraction of the crust along the southwest Washington profile is very heterogeneous, particularly across the accretionary prism into the Siletz terrane. Velocity variations on the order of 50-100% occur across distances of a few km. This dramatic structural variation makes for a time-consuming analysis of upper crustal velocity structure while also complicating the modelling of the deeper structure; tomographic inversion methods are thus the most effective means to analyze this complex portion of the velocity model. Any seismic tomography procedure requires an ability to compute travel-times and/or ray paths, stabilize and invert a large set of algebraic equations, and assess model reliability. We discuss these three aspects of the tomography problem separately.

Computing travel-times and ray paths. The computation of travel-times is prerequisite to inverting observed travel-times and thereby estimating the subsurface structure. We employ a finite-difference travel-time technique initially developed by Vidale (1988) and since extended by Vidale (1990) to perform more accurately in the presence of large velocity contrasts. In Vidale's (1988) method, travel-times are extrapolated outward from the source region to each point in the model (described by a finite-difference mesh). To handle structures with large velocity contrasts, Vidale (1990) added a recursive element to the algorithm that searches for refracting waves which may have been overlooked in the original algorithm. The resulting algorithm more accurately times refracted and turning waves for a moderate increase in computation time. Ray paths are computed by following the gradient in travel-time from the receiver to the source. To account for the large changes in elevation along the profiles (about 2 km of relief), we position the sources and receivers within a two-dimensional model, which is easily accommodated in the finite-difference grid. Most often, a receiver will not be located on a grid point of the model, so the arrival time to a receiver is estimated using plane-wave interpolation of the times surrounding the receiver.

Nonlinear inversion of arrival times for subsurface slowness. The relationship between a medium's slowness (inverse of velocity) distribution and a wave travel-time is nonlinear. Although the forward problem (computing times when given a velocity structure) may be solved with a number of approaches, solving the inverse problem (estimating the structure given a set of observed times) is more difficult. In media with small slowness variations, the relationship can be linearized using Fermat's principle, resulting in a much simpler mathematical relationship. Unfortunately, due to the strongly heterogeneous uppermost crust along the southwest Washington profiles, we cannot directly employ this simplification. We can, however, adopt the common approach of solving the nonlinear travel-time equations iteratively, using Fermat's principle in successive iterations to linearize each step towards a solution of the nonlinear problem. Clearly, in this iterative scheme, the initial velocity model plays an important role. We tested initial one-dimensional velocity structures based on a priori information from other studies of the area or areas with similar geologic characteristics. Because the dipping, high-velocity Juan de Fuca slab is associated with head waves along its top, we employed a two-dimensional starting model guided by MCS images of the descending slab (e.g., Flueh at al., 1997).

We discretize the velocity structure using constant slowness cells and represent the i^{th} slowness model using a vector notation $\mathbf{s}_i$. At each iteration, the relationship between the travel-times and the slowness perturbation, $\delta\mathbf{s}_{i+1} = \mathbf{s}_{i+1} - \mathbf{s}_i$, is

$$\mathbf{L}_i \delta\mathbf{s}_{i+1} = \delta\mathbf{t}_i \ . \tag{1}$$

$\mathbf{L}_i$ and $\delta\mathbf{t}_i$ are the path matrix and residual vector calculated using model $\mathbf{s}_i$. In general, seismic tomography problems are undetermined and ill-conditioned, and the direct inversion of (1) is very sensitive to small errors in the data. To produce reasonable estimates of the slowness, we must incorporate either geologic information or limit the possible solution to a certain class of models, such as the set of smoothest candidate models. This additional information may be incorporated by appending constraint equations to the system of equations relating the data and the model. We use a Laplacian smoothness criterion (Lees and Crosson, 1989) and the constraint equation for the cell located at x,z is of the form:

$$4s_{x,z} - s_{x-dx,z} - s_{x+dx,z} - s_{x,z-dz} - s_{x,z+dz} = 0 \tag{2}$$

where dx, and dz are the cell widths in the horizontal and vertical directions respectively. Additionally, minimum length constraints are necessary since the smoothest model criterion alone is sometimes inadequate to stabilize an inversion. The importance of smoothness, minimum length, and fitting the observed travel-times are varied using a minimum length weight, λ, and a smoothing weight, σ. The resulting equations are of the form

$$\begin{bmatrix} L_i \\ \sigma\Delta \\ \lambda I \end{bmatrix} \delta\mathbf{s}_{i+1} = \begin{bmatrix} \delta\mathbf{t}_i \\ 0 \\ 0 \end{bmatrix} \tag{3}$$

where $\mathbf{L}_i$ is a matrix of ray lengths and $\delta\mathbf{t}_i$ is the vector of travel-time residuals both evaluated using slowness estimate $\mathbf{s}_i$, I is the identity matrix (with the dimensions of the slowness model), Δ is a submatrix of Laplacian smoothness constraints. We solve (3) using the LSQR algorithm of Paige and Saunders (1982). Appropriate values for λ and σ are estimated using a trial-and-error approach.

Resolution. Resolution in tomography depends on three properties of the problem. The signal band width, the source-receiver distribution, and the velocity structure itself. Three approaches are usually adopted to investigate resolution in tomographic problems. The simplest is a hit count analysis. In this simple analysis, the number of rays sampling a given cell, or the sensitivity of all the travel-times to each node, are examined to identify regions of good coverage (and hence good resolution is inferred) and poor coverage. The second approach to resolution analysis is the construction of synthetic tests using the data distribution (Humphreys and Clayton, 1988). The synthetic test may be an attempt to construct point-spread functions, or may be an attempt to reconstruct the major features of the model simultaneously. The third common method of resolution analysis is the use of the resolution matrix constructed from an extension of linear inverse theory. Typically the diagonals of the resolution matrix are displayed, and a certain value is chosen to indicate "good" resolution. The resolution matrix is a construct well suited to the study of linear problems. However, the extension of this tool to nonlinear problems is always questionable, particularly when the solution is approached iteratively (Shaw and Orcutt, 1986). Each of the above resolution diagnostics depends on the velocity structure used to construct the resolution measures. Quantitatively connecting a hit count, synthetic test, or resolution matrix with the actual accuracy of the reconstructed image is not straight forward. A combination of these resolution indicators can provide some intuition into the resolving power of the data. We have chosen to use LSQR, and thus do not construct a formal resolution matrix; we use a combination of hit count and synthetic tests to estimate the degree of uniqueness of the solution.

We can get a rough idea of the maximum resolution of the data by examining the Fresnel Zones. The Fresnel Zone is calculated by computing the travel-time from the source to a point in the model and then on to the receiver. At the turning depth, the Fresnel Zone is about two kilometers wide, which indicates the practical limit on interpretation of the structure at depth. As expected, the Fresnel Zone is smaller at shallow depths where velocities are lower, and resolution should be better in these regions, provided adequate sampling by the data. Figure 6 contains the

coverage matrix for the final iterations of the inversions. The coverage for a node is calculated by summing the ray lengths of each ray path within a given cell.

The finite-difference travel-time inversion used to find the upper crustal velocity structure utilizes only first arrival times. To directly apply the inverted solution for the upper crust, we employed a finite-difference technique to forward-model crustal reflections, propagating though a 3-D velocity grid that contains the upper crustal model. We wrote the output from the first arrival travel-time inversion over a grid of input starting velocities, so that complexities in secondary phases that result from near-surface structures such as basins could be modelled as accurately as possible. The continental and oceanic PmP reflections were modeled first, and then the deep slab reflections were modeled once a crustal velocity structure was established. As a final step, Pn arrivals were inverted through the solved crustal model.

The finite-difference algorithm of Vidale (1988, 1990) is extended to compute reflection travel times (Hole and Zelt, 1994). The technique was developed for use in three dimensions, and we thus apply it to correct for the crooked-line geometry of the on-land data collection; the reflector positions are projected onto a plane for display. The reflecting interface is defined as a sampled function of the horizontal coordinate, and is allowed to vary smoothly in depth. To begin the procedure, first arrival travel times are computed from the point source to the reflecting interface. Velocities below the reflector are defined to be equal to, or less than, velocities above in order to prevent waves transmitted through the interface from arriving as first arrivals at the reflector. The computed times at the reflecting interface are thus the times of the incident down-going wave. To allow a smooth reflector to exist between grid nodes in depth, the computed incident times at the grid nodes immediately above the reflector are used to analytically compute reflected times at the same nodes. Travel times to shallower grid nodes are replaced with large dummy values. This sampled travel time field is input into the finite-difference algorithm and travel times are computed upward from the base of the model. Previously computed times (in particular the large dummy values) are replaced by upgoing times if the upgoing times are earlier. In this manner, the incident travel times on the reflecting interface are used as a source to propagate the reflected wave upwards through the model. Travel times were fit to within ± 0.15 s of the picked events shown on the accompanying data archive. Because of the sometimes weak, discontinuous nature of the wide-angle reflections, we assess our potential picking errors to be within the ± 0.15 s range.

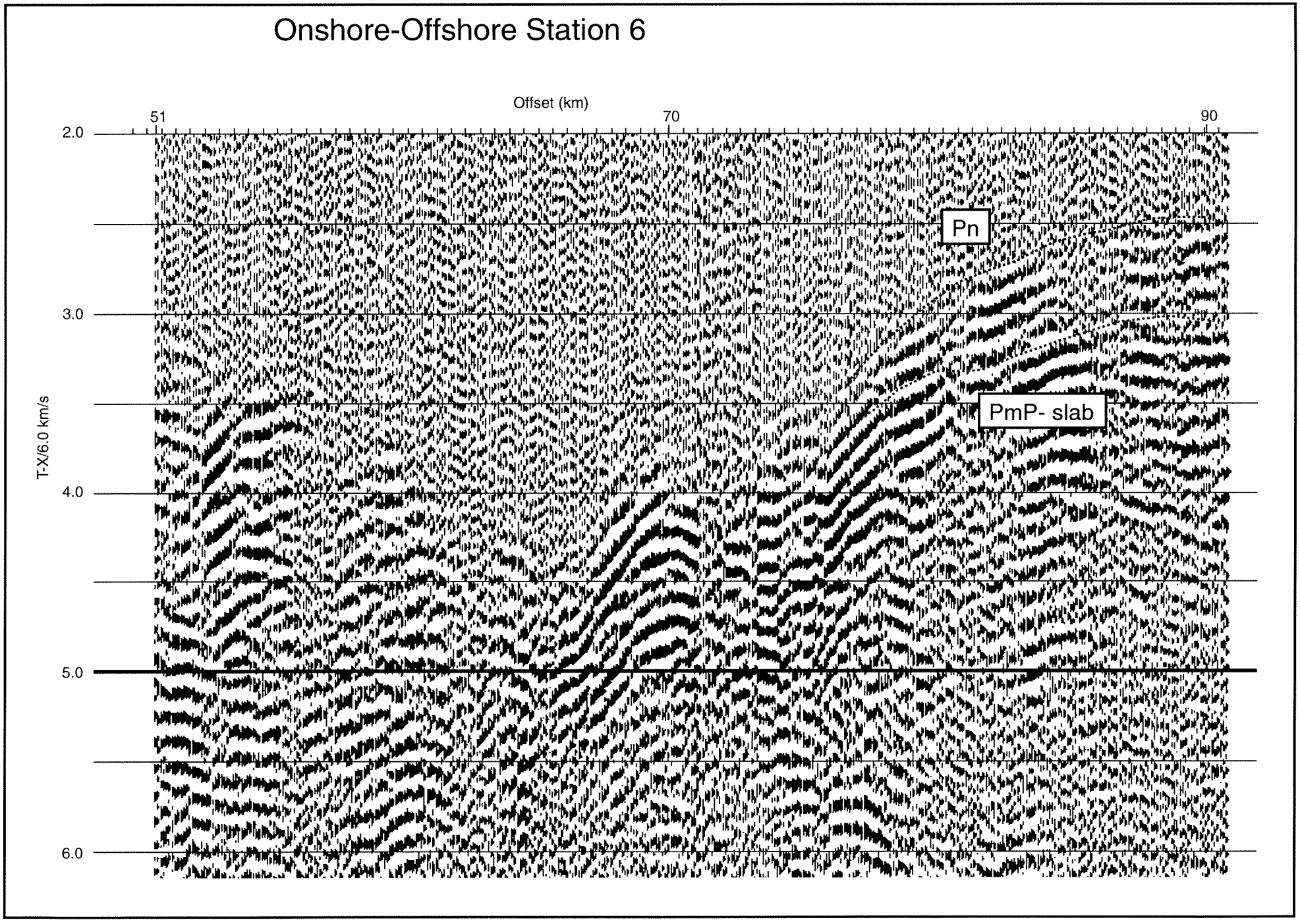

Figure 3. Receiver gather showing a PmP reflection from the slab and an upper mantle refraction (Pn)

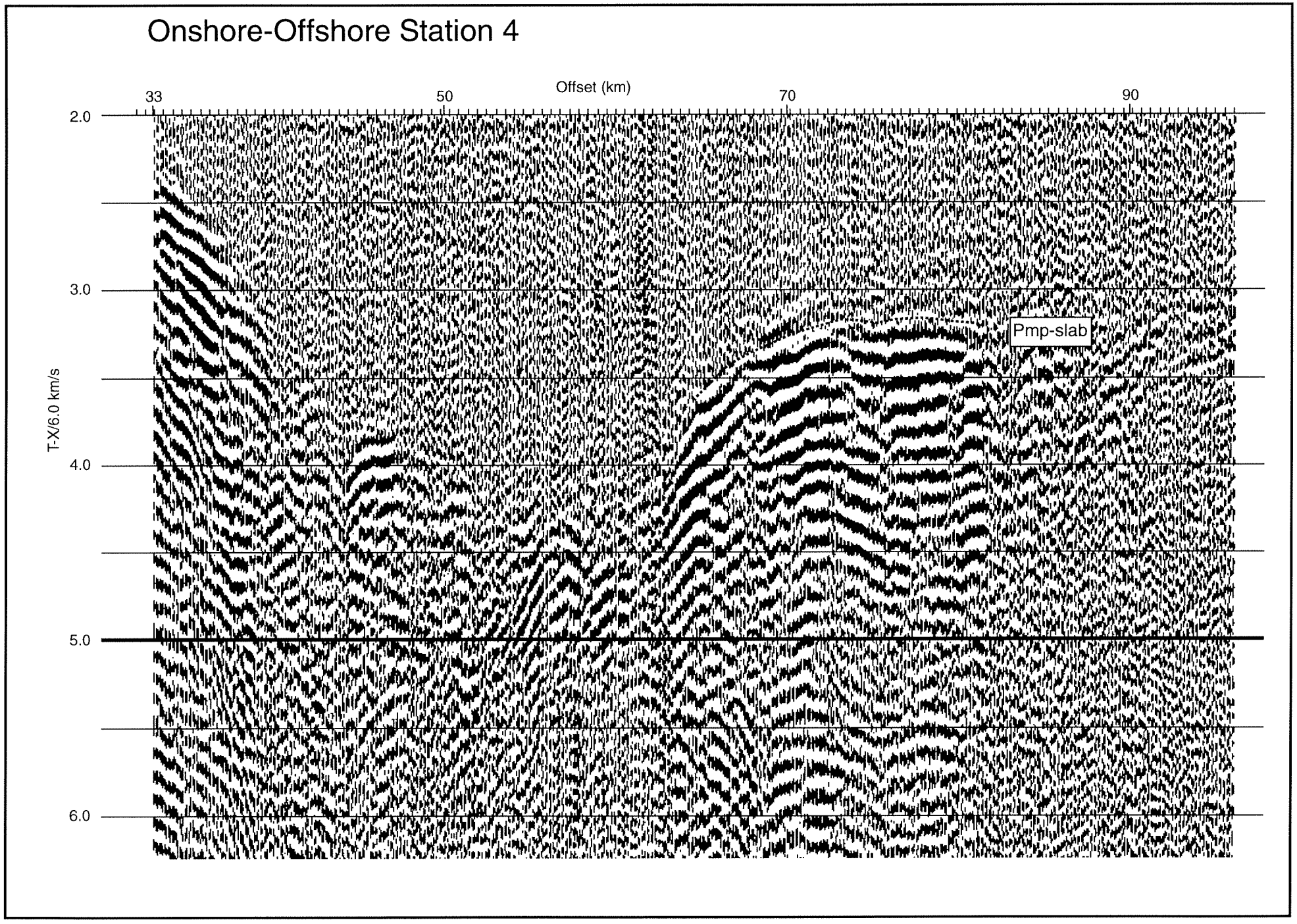

Figure 4. Receiver gather showing a PmP reflection from the slab.

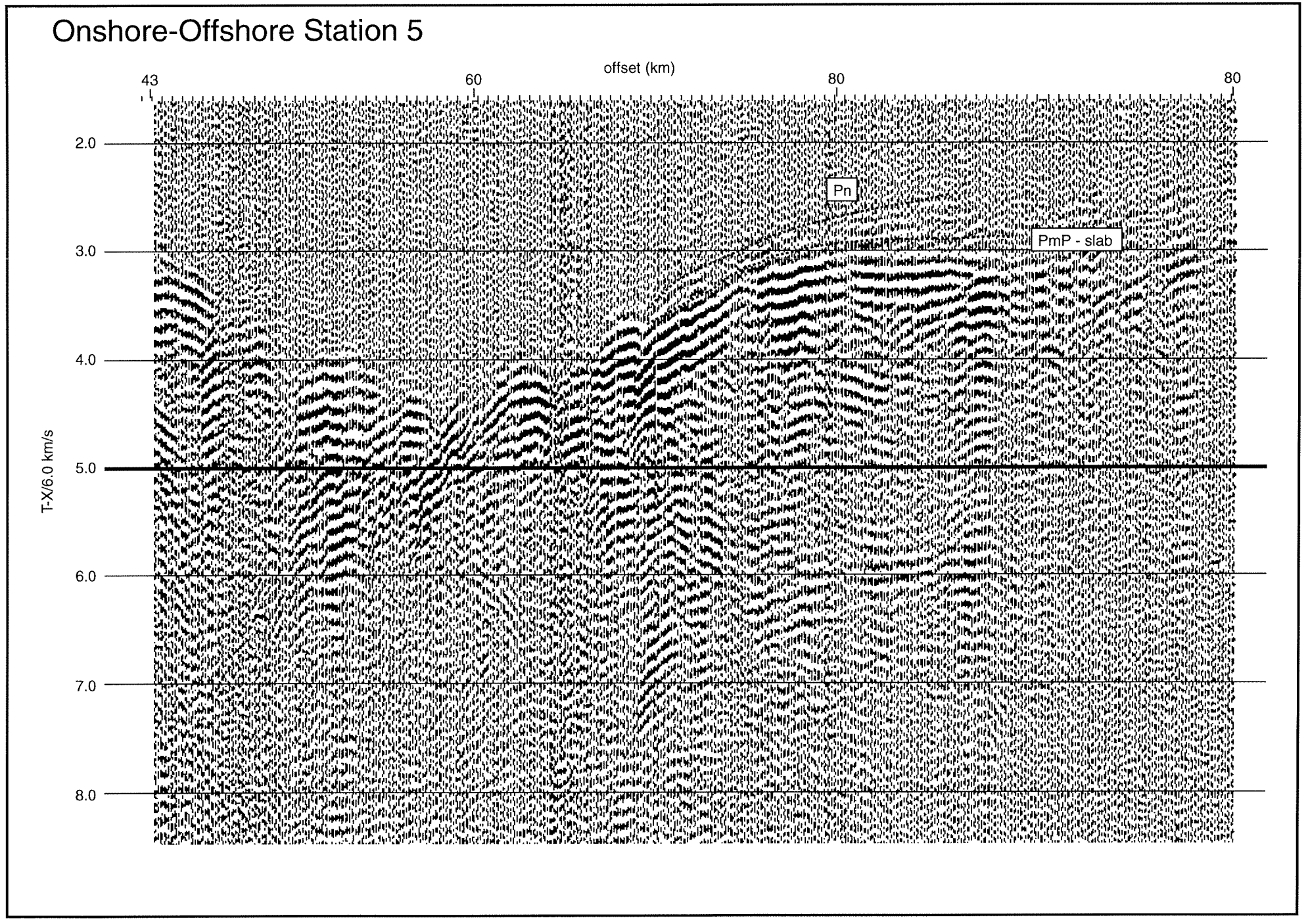

Figure 5. Receiver gather showing a PmP reflection from the slab and an upper mantle refraction (Pn)

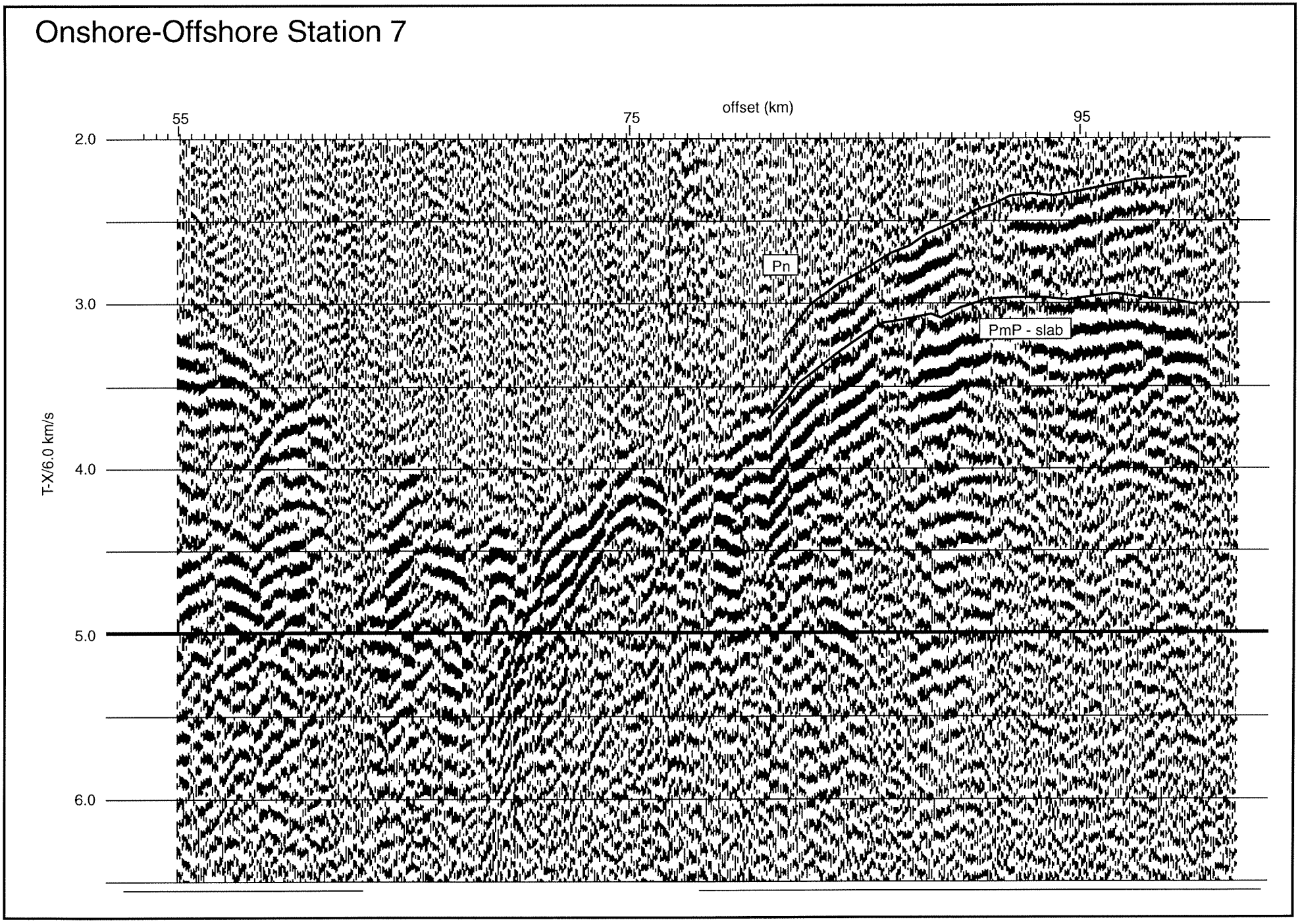

Figure 6. Receiver gather showing a PmP reflection from the slab and an upper mantle refraction (Pn)

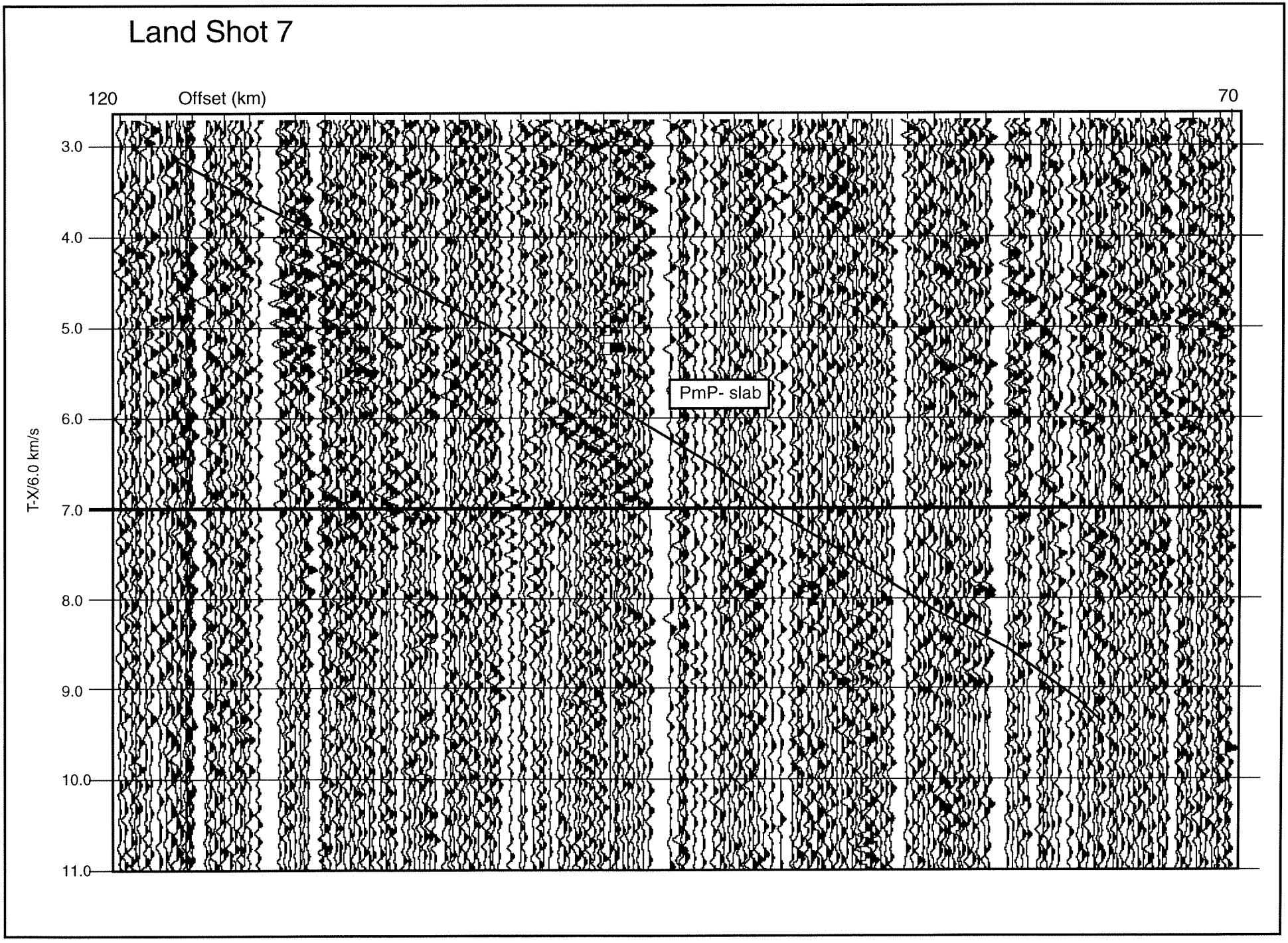

Figure 7. Shot gather showing a PmP reflection from the slab.

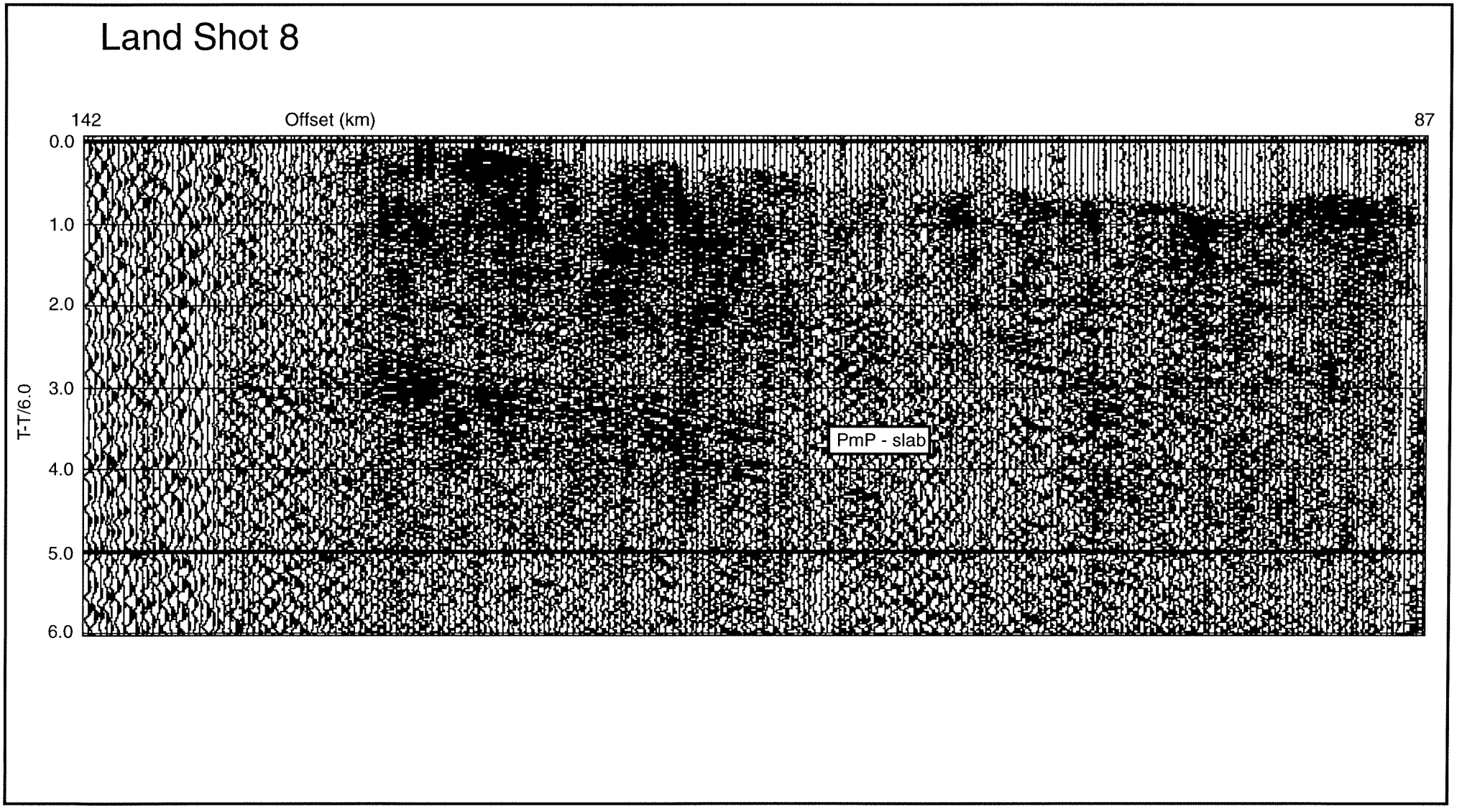

Figure 8. Shot gather showing a PmP reflection from the slab.

2. Data Showing Continental PmP Reflections

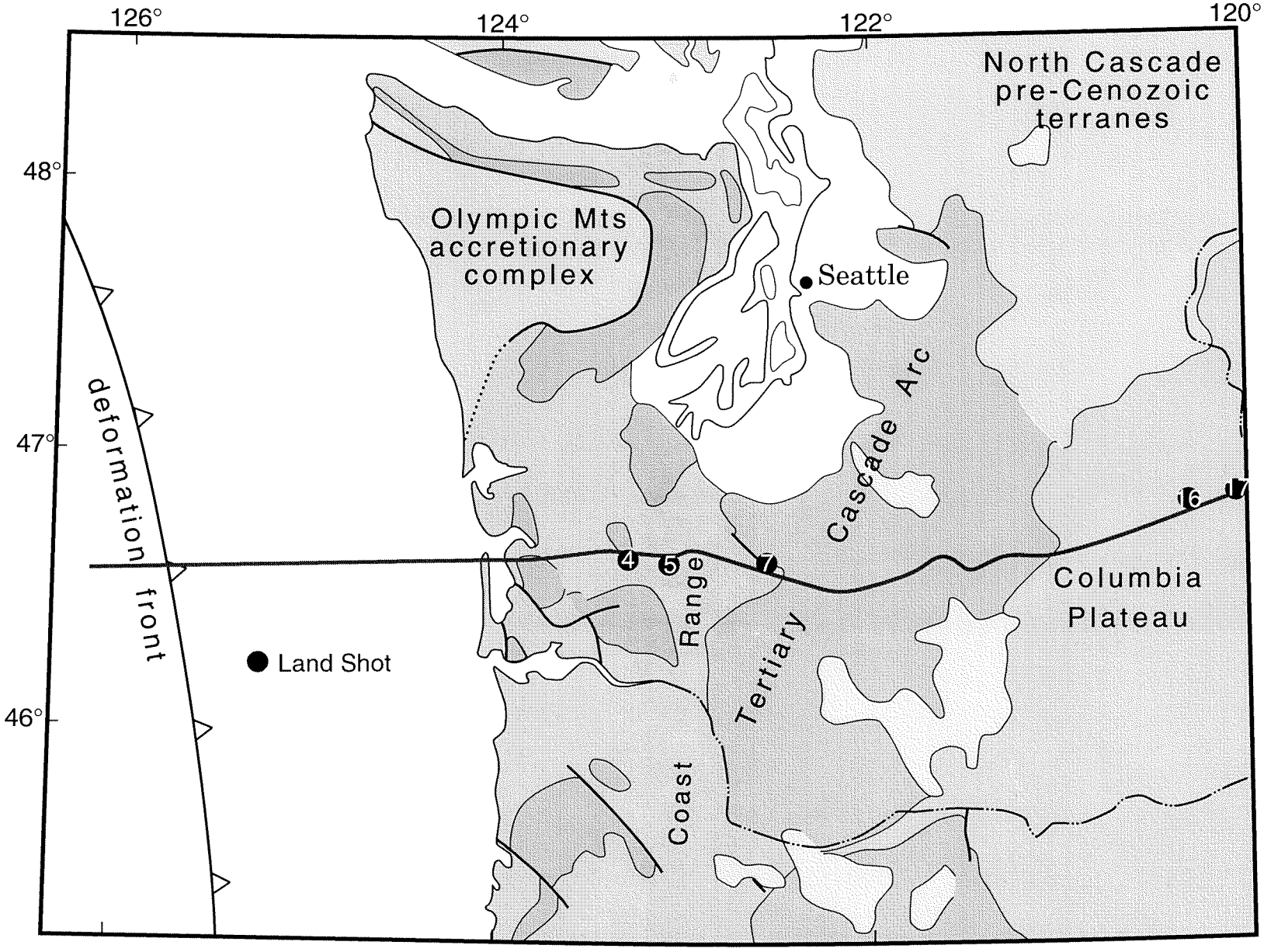

Figure 9. Locations of chemical shot points (data shown in Figures 10-14) used to model the thickness of the continental crust. More shots were used to model the shallow continental crust using first arrivals.

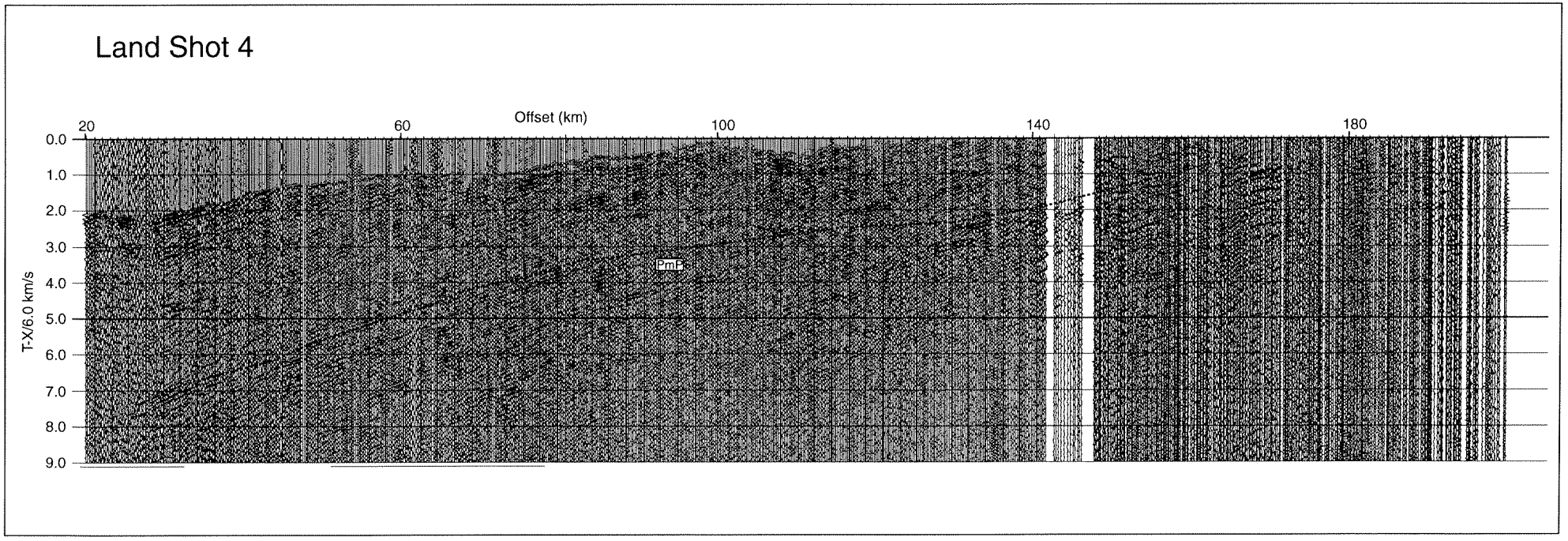

Figure 10. Shot gather showing a PmP reflection from the base of the crust.

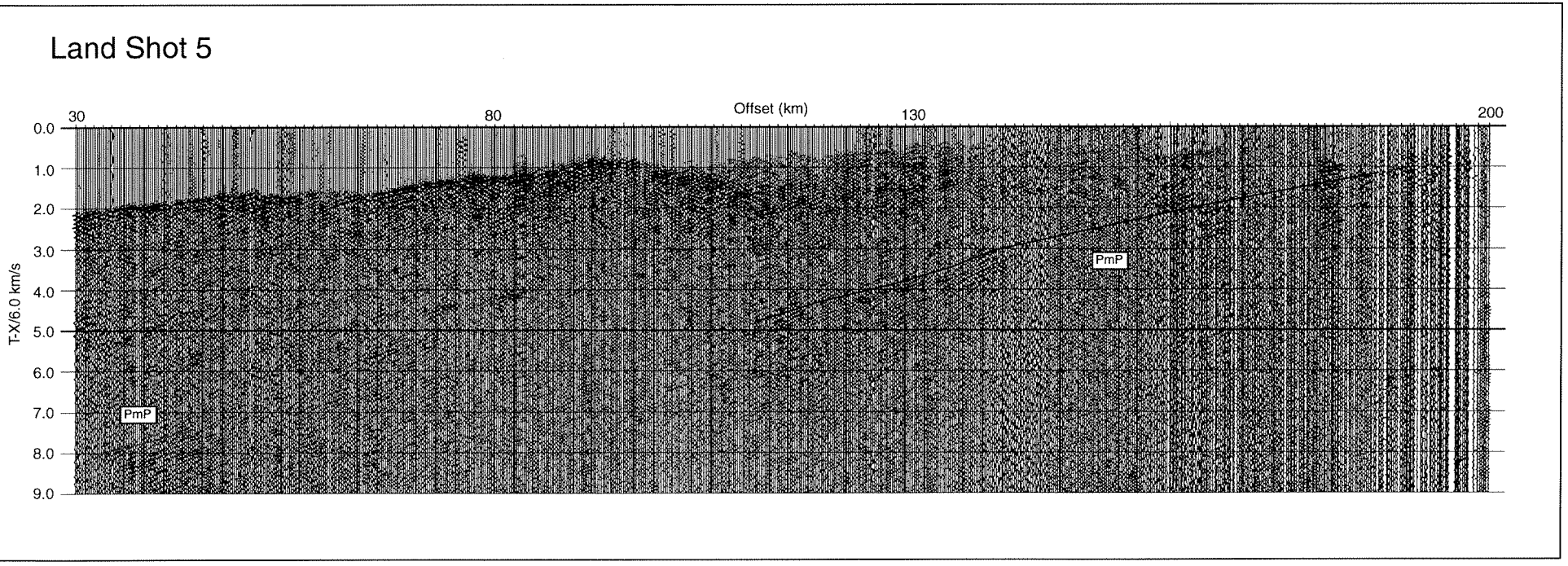

Figure 11. Shot gather showing a PmP reflection from the base of the crust.

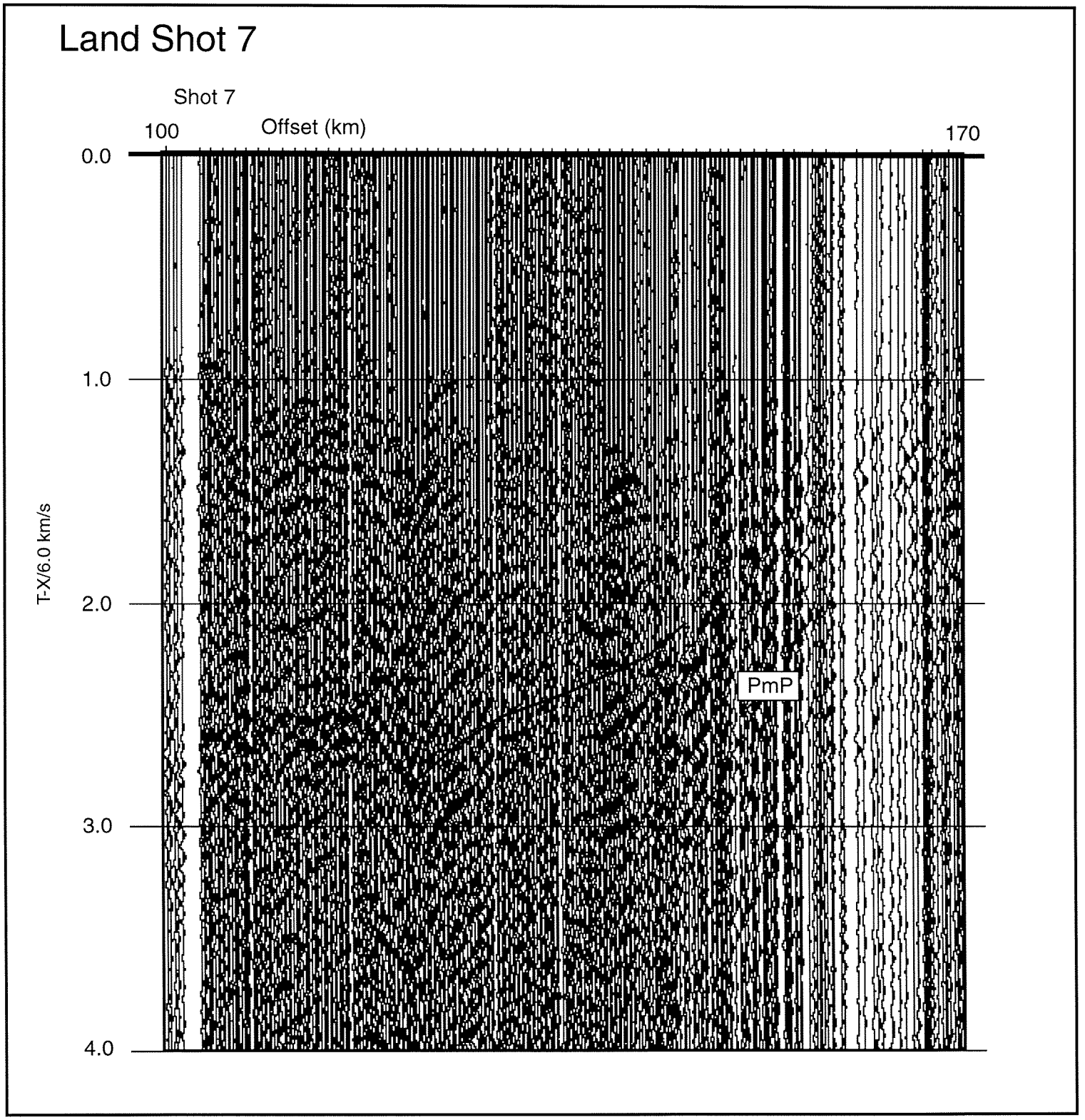

Figure 12. Shot gather showing a PmP reflection from the base of the crust.

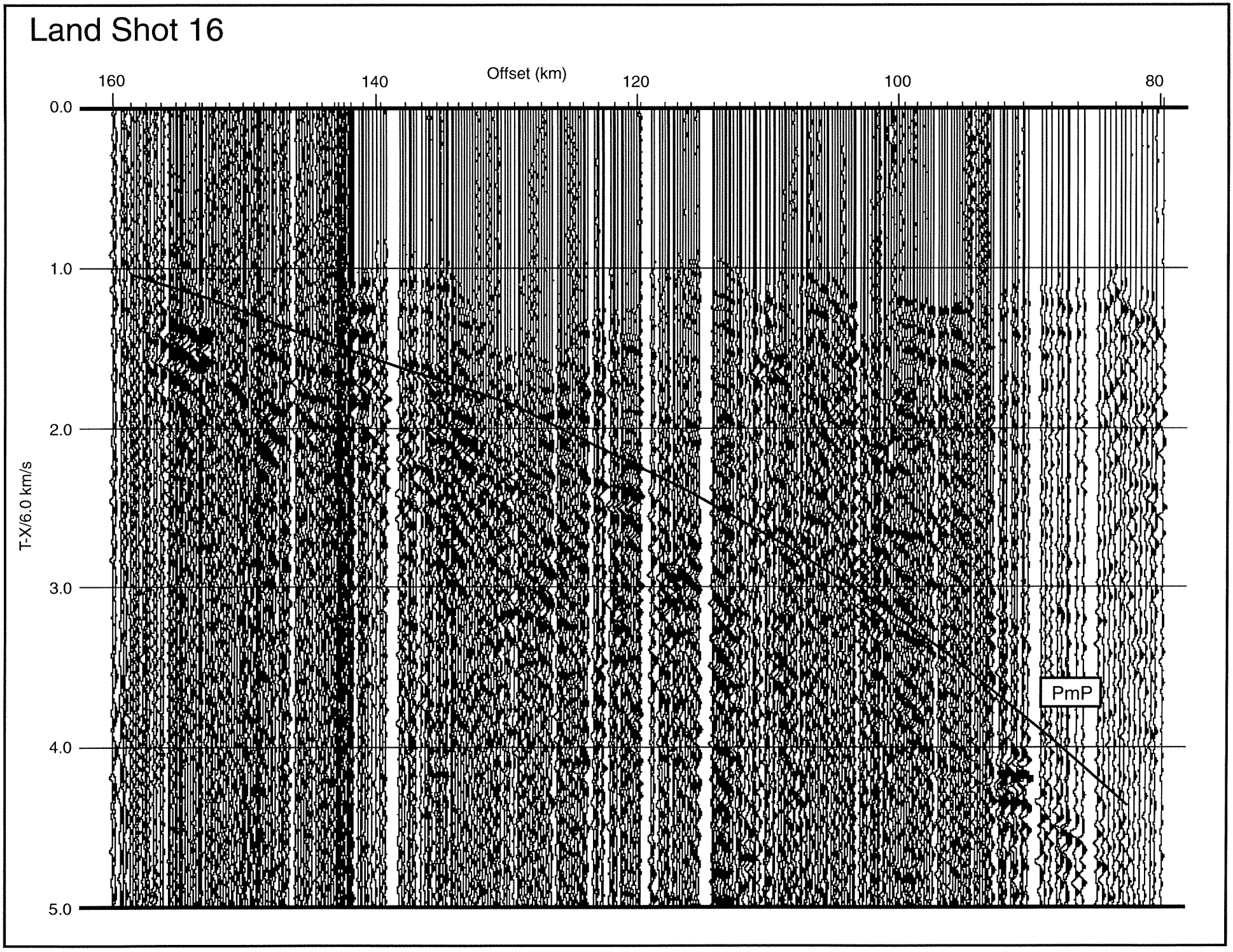

Figure 13. Shot gather showing a PmP reflection from the base of the crust.

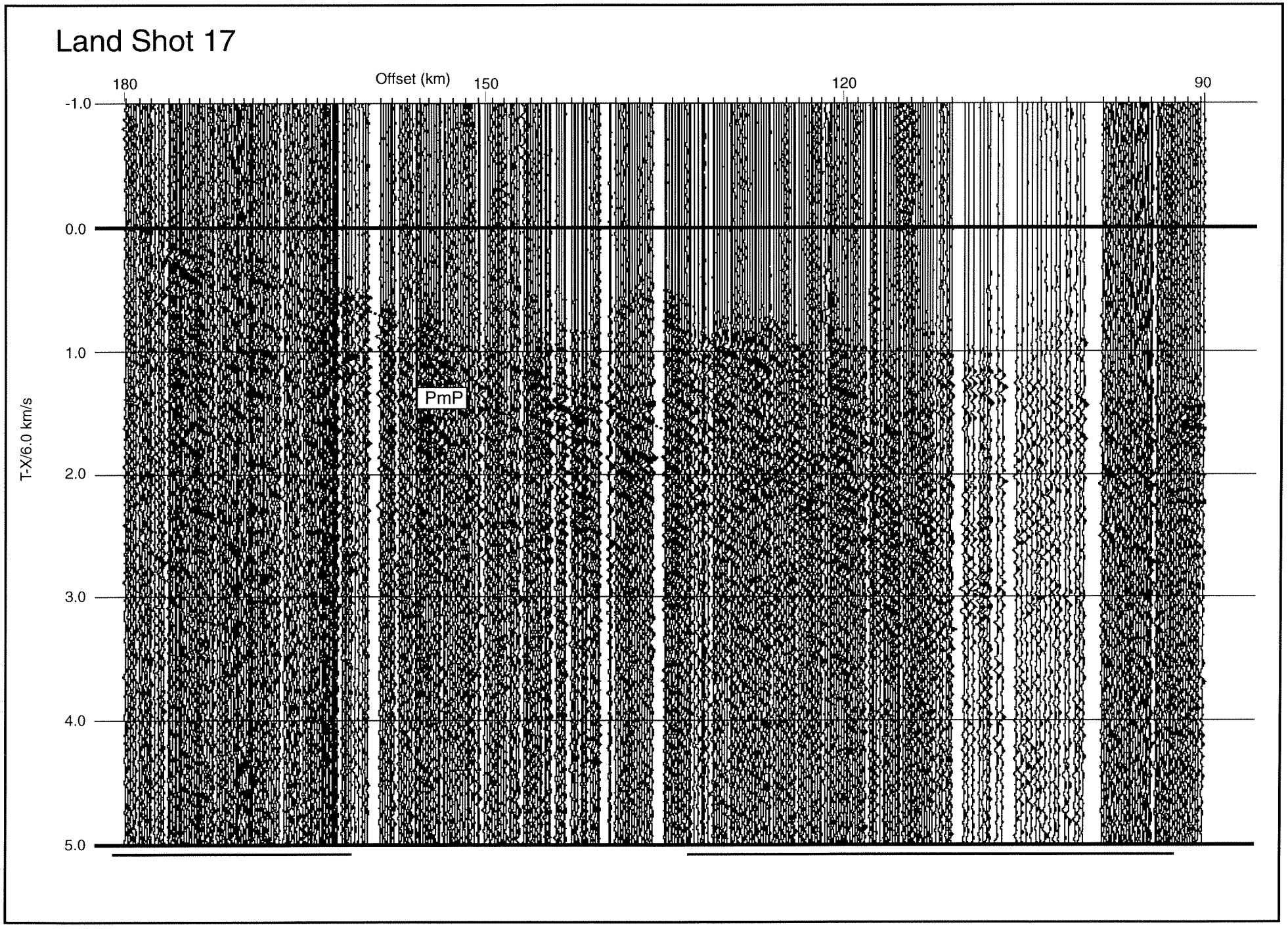

Figure 14. Shot gather showing a PmP reflection from the base of the crust.

3. Gravity Model

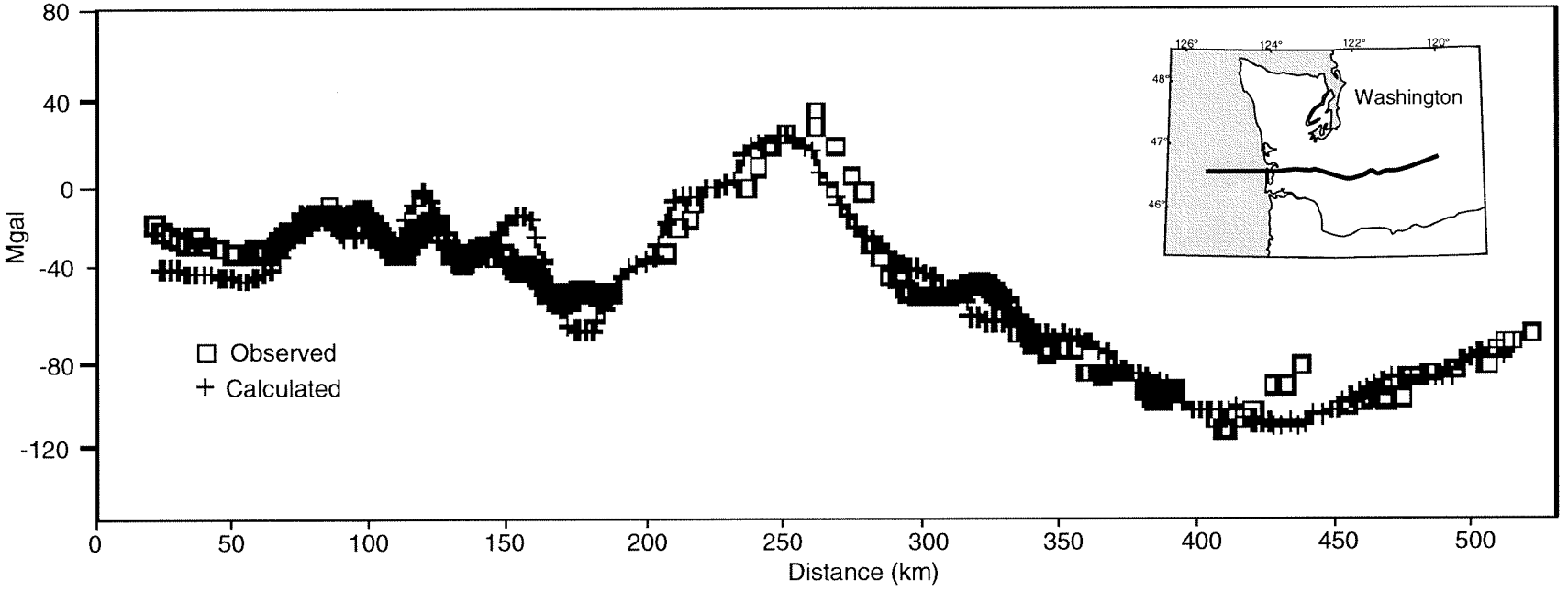

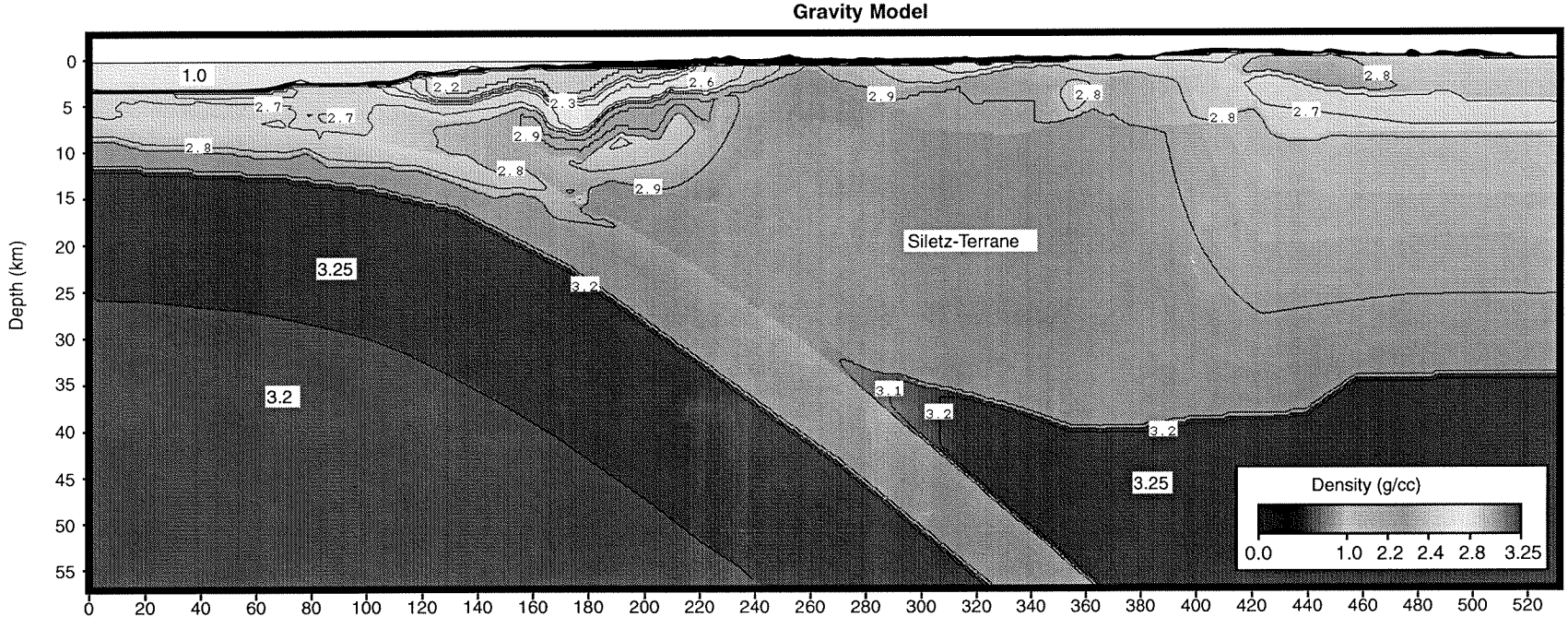

Figure 15

Figure 15. The gravity modeling was based on the velocity model. The philosophy of our gravity modeling was to test the velocity model with a simple velocity-density relationship. Because the purpose of the model is not interpretive, we did not tinker with crustal densities to make a perfect fit, but rather established that the basic shape of the velocity model is consistent with the observed gravity. We did introduce a higher velocity-density relationship in the mafic Siletz terrane and in the volcanic arc. The precise location of the profile was defined by the following points:

46.6489 -126.4486 (first airgun source)
46.6488 -125.3467 (100 km offshore)
46.5978 -124.0349 (coast)
46.5306 -122.1806 (Shot Point 8)
46.8306 -119.8542 (Shot Point 17)

The data comprising the profile were extracted from a CD-ROM (Hittelman et al., 1994) such that the data points were never more than 5 km from the profile. Additional points were extracted from a second CD-ROM (the GEODAS Marine Trackline Geophysics CD-ROM published by the U.S. National Geophysical Data Center) to provide additional coverage where necessary. After merging these data sets, the data points were edited to smooth the observed gravity profile, based on distance from and location relative to the profile, and to remove duplicate points. Where data coverage was good, maximum distance of the points from the profile was reduced to approximately 3 km. The data were referenced to the profile in order to correspond with the velocity model such that the first airgun source was 21.362 km from the origin and the coastline a distance of 206 km along the profile. The total length of the gravity profile is 530 km.

A subsurface model was generated based on the velocity model, such that the location of the bodies were defined by velocity contrasts. Since the offshore gravity data are Free Air and the onshore data are Bouguer corrected, the bathymetry offshore was incorporated into the model to bring the entire profile to the same reference datum. Bathymetry was extracted from the NOS hydrographic Survey data CD-ROM, also published by the U.S. National Geophysical Data Center. Additional constraints were provided to the model at the surface from the known geology (Walsh et al., 1983).

The model was used to generate a calculated gravity profile using a gravity profile modeling program based on the technique of Cady, 1980, which uses 2-1/2 dimensional bodies. The calculated and observed gravity profiles were compared and the subsurface model was updated in an iterative sense until the two profiles coincided. The velocity model provided constraints on

the densities of the bodies using known correlations between the two (Barton, 1986, Christensen and Mooney, 1995).

The final gravity model (Figure 4) corresponds relatively well to the velocity model and shows the shallow dip of the Juan de Fuca plate and the accretionary prism pushed up against a back-stop made up of the Crescent Formation. The density of the accretionary prism is a little high for such a low velocity feature, but lies within the range defined by Barton, (1986). Siletzia densities are quite high, similar to those of Finn, 1990. In contrast with the Finn, (1990), model is the absence of a low density body corresponding to the Southern Washington conductive corridor (Stanley et al., 1992). Such a body was not required by the model presented here.

REFERENCES

Barton, P. J., 1986, The relationship between seismic velocity and density in the continental crust-a useful constraint? Geophys. J. R. astr. Soc., 87,195-208.

Cady, W. J., 1980, Calculation of gravity and magnetic anomalies of finite-length right polygonal prisms. Geophysics 45, 1507-1512.

Christensen, N. I., and W. D. Mooney, 1995, Seismic velocity structure and composition of the continental crust: A global view. J. Geophys. Res., 81, 3047-3054.

Finn, C., 1990, Geophysical constraints on Washington convergent margin structure: Journal of Geophysical Research, v. 95, p.19,533-19,546.

Flueh, E., Fisher, M., Scholl, D., Parsons, T., ten Brink, U., Klaeschen, D., Kukowski, N., Trehu, A., Childs, J., Bialas, J., and Vidal, N., 1997, Scientific teams analyze earthquake hazards of the Cascadia subduction zone, EOS, p. 153-157.

Hole, J. A., Zelt, B. C., 3-D finite-difference reflection travel times, 1995, Geophysical Journal International, v. 121, p. 427-434.

Hittleman, A. M., D. T. Dater, R. W. Buhmann, and S. D. Racey, 1994, Gravity -1994 Edition CD_ROM User's Manual. United States Department of Commerce, National Geophysical Data Center.

Humphreys, E., and R. W. Clayton, 1988, Adaptation of back projection tomography to seismic travel time problems, Journal of Geophysical Research, v. 93, p. 1073-1085.

Lees, J. M., and R. S. Crosson, 1989, Tomographic inversion for three-dimensional velocity structure at Mount St. Helens using earthquake data, Journal of Geophysical Research, v. 94, p. 5716-5728, .

Paige, C.C. and M.A. Saunders, 1982, LSQR: An algorithm for sparse linear equations and sparse least squares, Trans. Math. Software, v. 8, p. 43-71.

Parsons, T., McCarthy, J., Kohler, W. M.., Ammon, C. J., Benz, H. M., Hole, J. A., and Criley, E. E., 1996, The crustal structure of the Colorado Plateau, Arizona: Application of new long-offset seismic data analysis techniques, Journal of Geophysical Research, v. 101, p. 11,173-11,194.

Shaw, P. R., and J. A. Orcutt, 1986, Waveform inversion of seismic refraction data and applications to young Pacific crust, Geophys. J. R. Astro. Soc., v. 82, p. 375-414.

Stanley, W.D., Gwilliam, W. J., Latham, G., and Westhusing, K., 1992, The southern Washington Cascades conductor-A previously unrecognized thick sedimentary sequence: American Association of Petroleum Geologists Bulletin, v. 76, p. 1569-1585.

Vidale, J. E., 1988, Finite-difference calculation of traveltimes, Bulletin of the Seismological Society of America, v. 78, p. 2062-2076.

Vidale, J. E., Finite-difference calculation of traveltimes in three dimensions, 1990, Geophysics, v. 55, p. 521-526.

Walsh, T. J., M. A. Korosec, W. M. Phillips, R. L. Logan, and H. W. Schasse, 1987, Geologic map of Washington-Southwestern quadrant. Washington division of geology and earth resources, Geologic map GM-34.